Comparing lattice Boltzmann simulations of periodic fluid flow in repeated micropore structures with longitudinal symmetry and asymmetry

Samuel J. Stephen[1] Barbara M. Johnston[2]
Peter R. Johnston[3]

(Received 14 February 2022; revised 7 June 2022)

Abstract

Pumping of a particulate suspension back and forth through a membrane of periodic axisymmetric pores results in no net flow of the fluid; however, the particles are transported along the pores from one side of the membrane to the other. The movement of the particles is dependent on the geometry of the pore walls. Current simulations for this problem utilise standard computational fluid dynamics techniques (e.g. finite element method, boundary element method). However, there are difficulties associated with applying these techniques to this

DOI:10.21914/anziamj.v63.17158, Published 2022-06-21, as part of the Proceedings of the 15th Biennial Engineering Mathematics and Applications Conference. ISSN 1445-8810. (Print two pages per sheet of paper.)

problem, such as the requirement of many spatial periods. The lattice Boltzmann method overcomes these disadvantages by utilising periodic boundary conditions, which are straightforward to implement. Flow simulations in longitudinally symmetric and asymmetric pores with various Reynolds numbers are compared. The importance of pore shape and viscous effects is showcased through streamline plots.

Contents

1 Introduction

Fluid flow through periodic micropore structures has widespread and multi-disciplinary applications, such as blood flow [11] and filtration [2]. A problem that has received recent attention is that of a particle-laden fluid pumped back and forth through a membrane of axisymmetric pores, where the diameter varies along its length in a periodic manner [12]. It is possible for the particles to be transported along the micropores despite no net fluid flow [6]. To achieve this phenomenon, it has been suggested that the pore geometry is

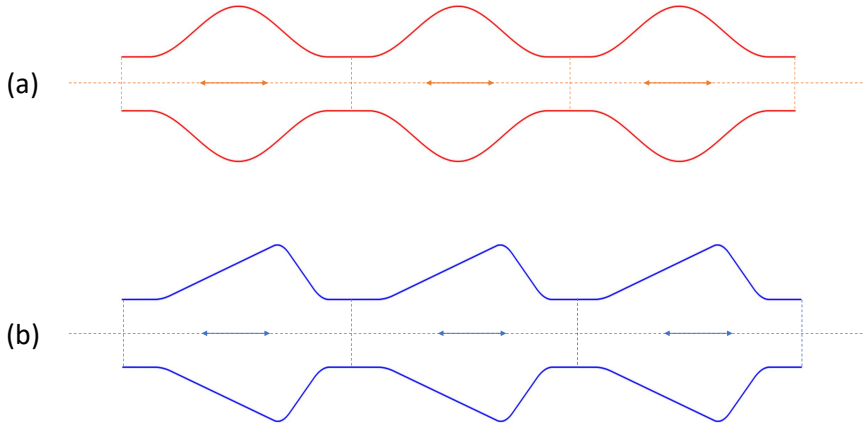

Figure 1: (a) Longitidunally symmetric micropore: sinusoidal profile. (b) Longitidunally asymmetric micropore: curved sawtooth profile.

the most influential factor; spatial periodicity with longitudinal asymmetry is thought to be required to facilitate particle transport [4, 7]. With this in mind, a direct comparison between symmetric and asymmetric micropores and their resulting flow fields would aid in understanding the differences that facilitate the movement of suspended particles. Figure 1 provides examples of symmetric and asymmetric pore profiles.

Before we can simulate periodic flow in both pore geometries, the fluid dynamics solver must be established. In prior modelling of this flow, standard boundary element computational fluid dynamics techniques were utilised [12, 6]. However, the implementation of these methods has some notable drawbacks when applied specifically to periodic flow in repeated micropore structures. This includes difficulty in incorporating viscosity dependence, as well as needing to consider many spatial periods in the computational domain [12, 6]. The lattice Boltzmann method (LBM) comes from an alternative framework that inherently considers fluid viscosity and has easy-to-implement boundary conditions that allow the computational domain to comprise only one spatial period [8]. Here, these periodic boundary conditions [8] are extended by

applying them to an LBM formulation in an axisymmetric coordinate system [13] to study flows resulting from the geometries described in Figure 1. In addition, numerical simulations are obtained using a specifically developed implementation in Python.

With viscosity dependence and relatively low computational cost, the LBM allows us to investigate not only the impact of pore shape, but also the effect that changing the Reynolds number has on the flow. This is done by measuring velocities and observing patterns in flow recirculation. In Section 2, relevant fluid dynamics background is presented, along with details of the LBM. Section 3 contains the process for preparing the simulation via developing the implementation and converting the physical problem into the lattice Boltzmann framework. Finally, Sections 4 and 5 discuss the results and summarise the findings, respectively.

2 Lattice Boltzmann method

2.1 Axisymmetric flow equations

Given the axisymmetry of the micropore strutctures mentioned, we are effectively simulating a 3D problem in 2D space due to the cross sections (see Figure 1) being rotationally symmetric. Hence, we consider the axial direction z and the radial direction r as part of a reduced 3D cylindrical coordinate system. The macroscopic governing equations are equivalent to the Navier–Stokes equations and, using Einstein summation, are

$$\frac{\partial u_i}{\partial t} + u_j \frac{\partial (u_i)}{\partial x_j} = -\frac{1}{\rho}\frac{\partial p}{\partial x_i} + \nu \frac{\partial^2 u_i}{\partial x_j^2} + \frac{\nu}{r}\frac{\partial u_i}{\partial r} - \frac{\nu u_i}{r^2}\delta_{ir}\,, \tag{1}$$

$$\frac{\partial u_j}{\partial x_j} = -\frac{u_r}{r}\,, \quad i,j \in \{z,r\}\,, \tag{2}$$

where t is time, p is pressure, ρ is fluid density, ν is kinematic viscosity, x_i and x_j represent direction, u_i and u_j are the velocity components and δ_{ir} is the Kronecker delta function.

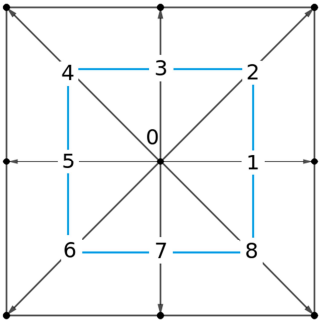

Figure 2: D2Q9 lattice velocity model.

2.2 2D lattice Boltzmann method

The LBM simulates the movement of local fluid densities, on a lattice consisting of cells, via collision and streaming processes, in accordance with a transport equation. Microscopic particle models, macroscopic variables and mesoscopic kinetic equations are combined to create a probabilistic model capable of determining the transport of particle population densities while maintaining highly accurate results when compared to alternate methods [3]. A generalised lattice Boltzmann equation takes the form

$$f_\alpha(\boldsymbol{x} + \boldsymbol{e}_\alpha \Delta t, t + \Delta t) - f_\alpha(\boldsymbol{x}, t) = \Omega(\boldsymbol{x}, t)\,, \tag{3}$$

where f_α is the distribution function of particles, $\boldsymbol{x}$ is the position vector, t is time, Δt is the time step, $\boldsymbol{e}_\alpha$ is the lattice velocity, α is a subscript to denote direction in the lattice velocity model and Ω is the collision operator. The left-hand side of equation (3) is denoted as the streaming step where $f_\alpha(\boldsymbol{x}, t)$ is propagated to $f_\alpha(\boldsymbol{x} + \boldsymbol{e}_\alpha \Delta t, t + \Delta t)$ and the choice of Ω defines the collision step. A typical lattice velocity model, which we utilize, is the D2Q9 (two dimensions, nine velocities) depicted in Figure 2. The D2Q9 considers eight outbound velocities to neighbouring cells as well as a rest velocity.

2.3 Axisymmetric lattice Boltzmann method

A standard 2D LBM would not suffice here as the axisymmetry needs to be taken into account. Zhou proposed the axisymmetric lattice Boltzmann

equation [13]

$$f_\alpha(\boldsymbol{x}+\boldsymbol{e}_\alpha\Delta t, t+\Delta t) - f_\alpha(\boldsymbol{x}, t) = -\tau_\alpha(f_\alpha - f_\alpha^{eq}) + w_\alpha\theta\Delta t + \frac{\Delta t}{\kappa c^2}e_{\alpha i}F_i\,, \quad (4)$$

where Δx is the lattice spacing, $c = \Delta x/\Delta t$ is the lattice speed, the weighting according to the D2Q9 is

$$\boldsymbol{w} = (4/9, 1/9, 1/36, 1/9, 1/36, 1/9, 1/36, 1/9, 1/36)\,, \quad (5)$$

the lattice unit velocity depicted in Figure 2 is defined by

$$\boldsymbol{e} = c((0,0),(1,0),(1,1),(0,1),(-1,1),(-1,0),(-1,-1),(0,-1),(1,-1))\,, \quad (6)$$

a constant is

$$\kappa = \frac{1}{c^2}\sum_\alpha e_{\alpha z}e_{\alpha z} = \frac{1}{c^2}\sum_\alpha e_{\alpha r}e_{\alpha r} = 6\,, \quad (7)$$

the source term is

$$\theta = -\frac{\rho u_r}{r}\,, \quad (8)$$

the force term in tensor form is defined as

$$F_i = -\frac{\rho u_i u_r}{r} - \frac{2\rho\nu u_i}{r^2}\delta_{ir}\,, \quad i \in \{z, r\}\,, \quad (9)$$

and the effective relaxation time is

$$\tau_\alpha = \begin{cases} \frac{1}{\tau}\,, & r = 0\,, \\ \frac{1}{\tau}\left(1 + \frac{(2\tau-1)e_{\alpha r}\Delta t}{2r}\right), & r \neq 0\,. \end{cases} \quad (10)$$

The relaxation time τ describes the characteristic time a system away from equilibrium relaxes to equilibrium [3]. The local equilibrium distribution is defined as [1]

$$f_\alpha^{eq} = w_\alpha\rho\left(1 + 3\frac{e_{\alpha r}u_r + e_{\alpha z}u_z}{c^2} + \frac{9}{2}\frac{(e_{\alpha r}u_r + e_{\alpha z}u_z)^2}{c^4} - \frac{3}{2}\frac{u_r^2 + u_z^2}{c^2}\right), \quad (11)$$

where u_r and u_z are the directional components of the macroscopic velocity and ρ is the fluid density. Furthermore, ρ and u_i are determined for every time step via conservation of mass and momentum, that is,

$$\rho = \sum_\alpha f_\alpha\,, \quad u_i = \frac{1}{\rho}\sum_\alpha e_{\alpha i} f_\alpha\,. \tag{12}$$

Along with τ_α, the $1/r$ terms in equations (8) and (9) are also set to zero when $r = 0$ to avoid singularities. This is possible through careful evaluation using l'Hopital's rule. This axisymmetric LBM recovers the Navier–Stokes equations and has been verified through many numerical simulations [13]. We reproduced these results as well as additional published results [12] to validate the implementation used in the simulations discussed in Sections 3 and 4.

3 Simulation details

3.1 Pressure gradient and boundary conditions

Figure 3 depicts the computational domain and boundary conditions of the simulations. The axisymmetry condition on the centreline streams outbound flow back inwards with the same axial velocity u_z but radial velocity $-u_r$.

We use a no-slip condition for the pore wall in the form of the interpolated bounce-back condition [9]. At the inlet and outlet of the pore, the generalised periodic boundary condition is used [8]. This condition streams outbound flow to the opposite end to simulate repeated geometries on both sides.

Lastly, a pressure gradient is incorporated into the force term from equation (9) to give the oscillatory flow in the axial direction. Thus, the force term now becomes

$$F_i = -\frac{\rho u_i u_r}{r} - \frac{2\rho\nu u_i}{r^2}\delta_{ir} + p_0 \cos\left(\frac{2\pi t}{T}\right)\delta_{iz}\,, \quad i \in \{z, r\}\,, \tag{13}$$

where p_0 is the maximum amplitude of pressure and T is the period.

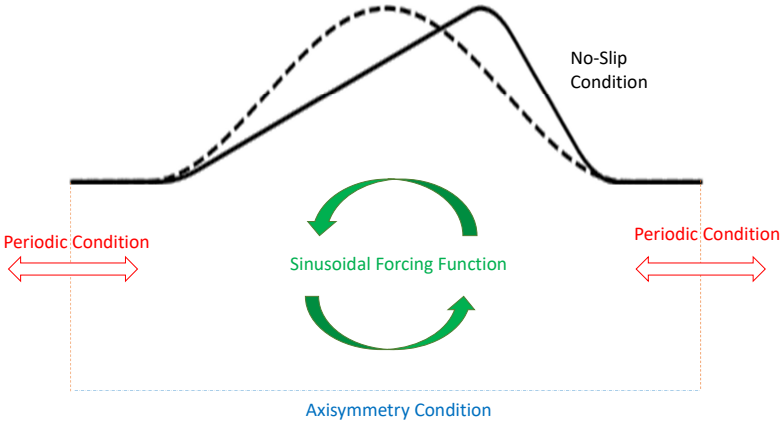

Figure 3: Computational domain, boundary conditions and pressure gradient.

3.2 Parameters

The Reynolds number is defined as

$$\mathrm{Re} = \frac{2U_c R}{\nu}, \tag{14}$$

where U_c is the characteristic velocity and R is the radius of the expansion region of the pore. Along with the pore geometry, Re is a unique identifier of the system. We also have the following relationship between viscosity and relaxation time [13]:

$$\nu = \frac{c^2 \Delta t(2\tau - 1)}{6}. \tag{15}$$

Therefore, by setting the parameters mentioned in equations (14) and (15), we can control the Re of the flow simulation. This grants access to flow regimes that were previously intractable for other fluid dynamics techniques applied to this problem.

For all simulations, we assign the values $\Delta x = \Delta t = 1$, $\tau = 0.6$, $R = 20$, with U_c allocated a value depending on the desired Re. This parameter set is consistent with published simulations [13] and is chosen because it balances

accuracy and numerical stability, as well as being simple. We set $T = 1200$ (representing time steps in a period), $p_0 = 0.001$ and $\rho = p_0 R^2/4U_c\nu$. This choice of the average fluid density ρ maintains consistency with Womersley flow characteristics [13].

To avoid compressible fluid effects which lead to numerical instability and inaccuracies, it is required that the Mach number

$$\mathrm{Ma} = \frac{\sqrt{3}U_{lb}\Delta t}{\Delta x}, \tag{16}$$

where U_{lb} is the characteristic velocity in the lattice Boltzmann system, is kept low (i.e. Ma< 0.3) [9]. Therefore, by setting $\Delta x = \Delta t = 1$ the requirement is satisfied by keeping the velocity sufficiently small for all simulations.

By comparing analytical and numerical solutions for Womersley flow in a straight tube, it was found that increasing the number of cells and time steps in the period led to higher accuracy across all tests. It has also been found in a separate mesh independence study, that simulations of longitudinally symmetric and asymmetric geometries converge smoothly as mesh resolution increases. These studies were completed to ensure accuracy of the independently developed axisymmetric lattice Boltzmann implementation we use here.

4 Results

The simulations were run for sufficiently many periods to observe convergent and repeated fluid behaviour. In total, six simulations were produced: the longitudinally symmetric and asymmetric pores with Re $= 10, 100$ and 1000.

Across all simulations, the pressure term in equation (13) is at its maximum positive value p_0 at the start of the period ($t/T = 0$) and reaches the maximum negative pressure $-p_0$ halfway through the period ($t/T = 0.5$). After maximum pressure along the z-axis, a jet of maximum velocity forms in the constricted regions (inlet and outlet), while velocity is noticeably lower

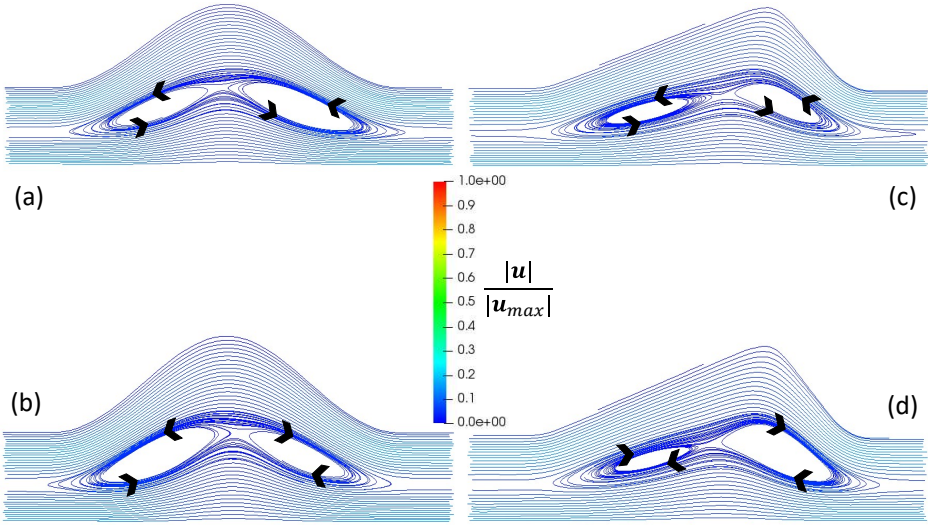

Figure 4: Re = 10 (a) symmetric pore, t/T ≈ 0.46; (b) symmetric pore, t/T ≈ 0.96; (c) asymmetric pore, t/T ≈ 0.46; (d) asymmetric pore, t/T ≈ 0.96.

in the expansion region. As t/T increases from 0 to 0.5 the pressure inverts, u_z drops and the flow reverses. Areas of zero velocity form which act as centres of rotation for the flow. Recirculation also occurs near the end of the period when the pressure term increases back to the maximum. However, the flow is reversed travelling in the negative axial direction to positive instead of the opposite case earlier in the period.

We do not present velocity vector fields here. While there are differences in the velocity vector fields for different pore shapes and Re values, they are more subtle than the streamline flow visualisations in Figures 4, 5 and 6 which represent uniform/uninterrupted flow along z. This means that breaks in the streamlines indicate zones of recirculation. The time points for the plots are chosen to best represent key instances of recirculation across the different Re systems.

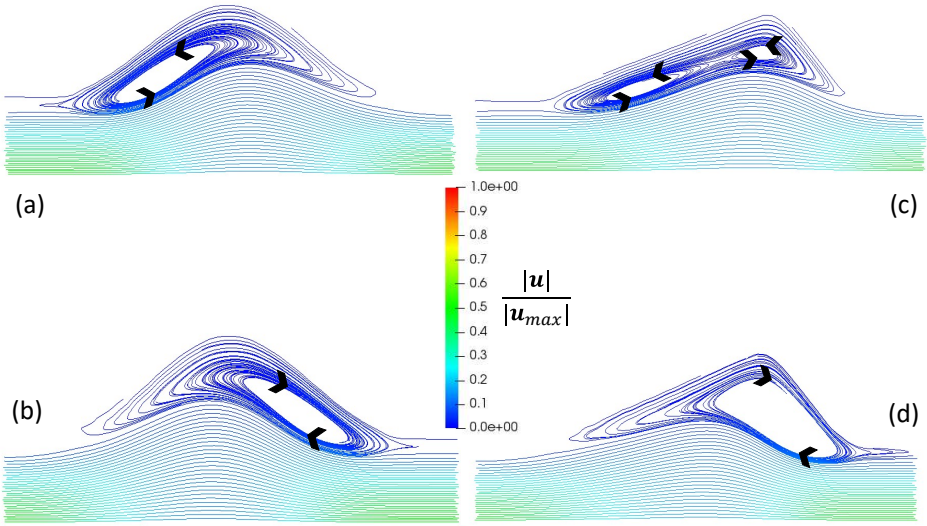

Figure 5: Re = 100 (a) symmetric pore, t/T ≈ 0.40; (b) symmetric pore, t/T ≈ 0.90; (c) asymmetric pore, t/T ≈ 0.40; (d) asymmetric pore, t/T ≈ 0.90.

Figure 4 shows streamline plots of periodic flow in symmetric and asymmetric pores with Re = 10. The colour map describes magnitudes of $\mathbf{u}$ scaled by the maximum $\mathbf{u}_{\max}$ across both pore profiles for Re = 10. The black arrows indicate the direction of flow. The time points chosen represent recirculation in both directions separated by exactly half the period. The symmetric profile streamlines are approximately symmetric (also exhibited in Figures 5 and 6), whereas the same cannot be said in the case of the asymmetric profile. Across both pore shapes for fixed time points, the vortices appear to be slightly different in size and position. However, the overall trend in the paths of these recirculation zones are similar; recirculation starts in the expansion region and separates into two zones while moving toward the centreline.

In Figure 5 for Re = 100 a key distinction between the two pore shapes arises. For the asymmetric pore in the transition from forward to backwards flow

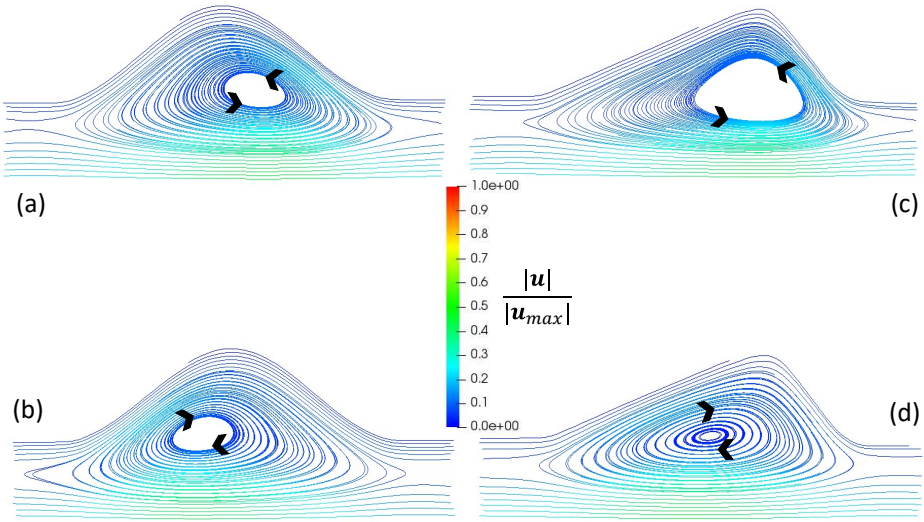

Figure 6: $\mathrm{Re} = 1000$ (a) symmetric pore, $t/T \approx 0.42$; (b) symmetric pore, $t/T \approx 0.92$; (c) asymmetric pore, $t/T \approx 0.42$; (d) asymmetric pore, $t/T \approx 0.92$.

(Figure 5c), two recirculation zones appear in the expansion region around the maximum radius. However, in the transition from backwards to forward flow (Figure 5d), there is only one recirculation zone. For the symmetric pore profile only one recirculation zone forms at both time points.

Lastly, Figure 6 showcases the recirculation zones for simulations with $\mathrm{Re} = 1000$. Recirculation starts as early as $t = 200$, which is at least 200 time steps earlier than the lower Re simulations. The jets of maximum velocity extend across the whole main channel which gives rise to areas of rotating flow large enough to occupy the majority of the pore.

5 Conclusion

To summarise: we simulated oscillatory fluid flow in longitudinally symmetric and asymmetric micropore structures for various Reynolds numbers by utilising an independently developed and verified axisymmetric LBM implementation. Not only did we observe recirculation zones of different sizes and trajectories, but we also noticed the number of vortices change due to geometric asymmetry (Figure 5). Conversely, the symmetric profile produced identical recirculation zones for the decline versus rise in axial pressure. This indicates that asymmetry in the pore allows asymmetry in the flow. It is precisely this flow asymmetry that allows for particle transport observed in physical experiments [5]. Additionally, it has been shown experimentally [10] that the size of recirculation zones increases when Re is increased and his is consistent with the simulations presented here.

The next step is to produce a more comprehensive simulation by approximating suspended particle transport within the flow fields.

References

[1] P. L. Bhatnagar, E. P. Gross, and M. Krook. "A model for collision processes in gases. I. Small amplitude processes in charged and neutral one-component systems". In: *Phys. Rev.* 94.3 (1954), p. 511. DOI: 10.1103/PhysRev.94.511 (cit. on p. C74).

[2] W. R. Bowen and F. Jenner. "Theoretical descriptions of membrane filtration of colloids and fine particles: An assessment and review". In: *Adv. Colloid Interface Sci.* 56 (1995), pp. 141–200. DOI: 10.1016/0001-8686(94)00232-2 (cit. on p. C70).

[3] S. Chen and G. D. Doolen. "Lattice Boltzmann method for fluid flows". In: *Ann. Rev. Fluid Mech.* 30 (1998), pp. 329–364. DOI: 10.1146/annurev.fluid.30.1.329 (cit. on pp. C73, C74).

[4] R. L. C. Cisne, T. F. Vasconcelos, E. J. R. Parteli, and J. S. Andrade. "Particle transport in flow through a ratchet-like channel". In: *Microfluid. Nanofluid.* 10 (2011), pp. 543–550. DOI: 10.1007/s10404-010-0688-y (cit. on p. C71).

[5] J. A. Deiber and W. R. Schowalter. "Flow through tubes with sinusoidal axial variations in diameter". In: *AIChE J.* 25.4 (1979), pp. 638–645. DOI: 10.1002/aic.690250410 (cit. on p. C81).

[6] N. Islam. "Fluid flow and particle transport through periodic capillaries". In: *Bull. Aust. Math. Soc.* 96.3 (2017), pp. 521–522. DOI: 10.1017/S0004972717000739 (cit. on pp. C70, C71).

[7] C. Kettner, P. Reimann, P. Hänggi, and F. Müller. "Drift ratchet". In: *Phys. Rev. E* 61.1 (2000), p. 312. DOI: 10.1103/PhysRevE.61.312 (cit. on p. C71).

[8] S. H. Kim and H. Pitsch. "A generalized periodic boundary condition for lattice Boltzmann method simulation of a pressure driven flow in a periodic geometry". In: *Phys. Fluids* 19.10 (2007), p. 108101. DOI: 10.1063/1.2780194 (cit. on pp. C71, C75).

[9] T. Krüger, H. Kusumaatmaja, A. Kuzmin, O. Shardt, G. Silva, and E. M. Viggen. *The lattice Boltzmann method: Principles and practice*. Vol. 10. Graduate Texts in Physics. Springer International Publishing, 2017, pp. 978–3. DOI: 10.1007/978-3-319-44649-3. (Cit. on pp. C75, C77).

[10] G. Leneweit and D. Auerbach. "Detachment phenomena in low Reynolds number flows through sinusoidally constricted tubes". In: *J. Fluid Mech.* 387 (1999), 129–150. DOI: 10.1017/S0022112099004619 (cit. on p. C81).

[11] M. Sakthivel and K. Anupindi. "An off-lattice Boltzmann method for blood flow simulation through a model irregular arterial stenosis: The effects of amplitude and frequency of the irregularity". In: *Phys. Fluids* 33.3 (2021), p. 031912. DOI: 10.1063/5.0044948 (cit. on p. C70).

[12] T. Sikdar, N. J. Pinky, A. Roy, S. S. Hossain, and N. Islam. "Oscillating flow of viscous incompressible fluid through sinusoidal periodic tube at low Reynolds number". In: *Int. J. Fluid Mech. Therm. Sci.* 6.1 (2020), pp. 9–18. DOI: 10.11648/j.ijfmts.20200601.12 (cit. on pp. C70, C71, C75).

[13] J. G. Zhou. "Axisymmetric lattice Boltzmann method revised". In: *Phys. Rev. E* 84.3 (2011), p. 036704. DOI: 10.1103/PhysRevE.84.036704 (cit. on pp. C72, C74, C75, C76, C77).

Author addresses

1. **Samuel J. Stephen**, Queensland Micro- and Nanotechnology Centre, Griffith University, Nathan, Queensland 4111, AUSTRALIA.
mailto:samuel.stephen@griffith.edu.au
orcid:0000-0003-2884-2923

2. **Barbara M. Johnston**, School of Environment and Science, Griffith University, Nathan, Queensland 4111, AUSTRALIA.

3. **Peter R. Johnston**, School of Environment and Science, Griffith University, Nathan, Queensland 4111, AUSTRALIA.